Highly efficient affinity anchoring of gold nanoparticles on chitosan nanofibers via dialdehyde cellulose for reusable catalytic devices

Highly efficient affinity anchoring of gold nanoparticles on chitosan nanofibers via dialdehyde cellulose for reusable catalytic devices

Alžběta Důbravová[a], Monika Muchová[a], David Škoda[a], Lenka Lovecká[a], Lucie Šimoníková[b], Ivo Kuřitka[a], Jan Vícha[a,*], Lukáš Münster[a,*]

[a]*Centre of Polymer Systems, Tomas Bata University in Zlín, tř. Tomáše Bati 5678, 760 01 Zlín, Czech Republic*

[b]*Department of Chemistry, Faculty of Science, Masaryk University, Kotlarska 2, 611 37 Brno, Czech Republic*

[*]*Corresponding author: E-mail addresses: jvicha@utb.cz (J. Vícha), munster@utb.cz (L. Münster).*

ABSTRACT

Polysaccharides are often utilized as reducing and stabilizing agents and as support in the synthesis of gold nanoparticles ($AuNPs$). However, using approaches like spin coating or dip coating, $AuNPs$ are generally bound to the support only by weak interactions, which can lead to decreased stability of the composite. Here, a two-stage approach for the preparation of composites with covalently anchored $AuNPs$ is proposed. First, 5 nm $AuNPs$ with high catalytic activity for the reduction of 4-nitrophenol ($TOF = 15.8$ min^{-1}) were synthesized and stabilized using fully oxidized and solubilized 2,3-dialdehyde cellulose (DAC). Next, the carbonyl groups in the shell of prepared nanoparticles were used to tether AuNPs to chitosan nanofibers with quantitative efficacy in a process that we termed "affinity anchoring". Schiff bases formed during this process were subsequently reduced to secondary amines by borohydride, which greatly improved the stability of the composite in the broad pH range from 3 to 9. The catalytic efficacy of the resulting composite is demonstrated using a model catalytic device, showing high stability, fast conversion rates, and direct reusability.

Keywords: Gold nanoparticles, dialdehyde cellulose, chitosan, nanofibers, electrospinning, catalysis

1. Introduction

A thousand years ago, gold nanoparticles ($AuNPs$) were already being used in China as an inorganic dye to introduce red color into porcelain (**Cao & Wang, 2011**). Nowadays, their applications have broadened to involve many fields, e.g. pharmacy and medicine (**Medina et al., 2007; Tiwari et al., 2011; Zhang, 2015**), the food industry (**Hasanova et al., 2022; Maddaloni et al., 2022; Sadanandan et al., 2023**), and chemical technology (**Bhatti et al., 2022; Gupta et al., 2023; Yuan, Ge, et al., 2023; Yue et al., 2023**). The wide application range of $AuNPs$ is possible due to their different sizes and shapes, which cause the required variances in their properties. For instance, to maximize the catalytic performance of $AuNPs$, the nanoparticles should be less than 10 nm in diameter, because catalytic efficacy drops dramatically for larger particles (**Corma & Garcia, 2008**). The nature of the preparation

method and other reaction parameters (pH, temperature, reaction time, reagent concentration) determine the shape, morphology, and size of the prepared $AuNPs$ (**Chen et al., 2008; S. Li et al., 2015; Xiao et al., 2020**). Hence, the key to unlocking the full application potential of $AuNPs$ lies in the design of their synthesis. The most common method for $AuNPs$ preparation is the Turkevich method, based on the citrate reduction of gold salts (**Enustun & Turkevich, 1963**). Although this method is green, controllable, and efficient, the prepared AuNPs must be stabilized by suitable capping agents to prevent aggregation in different media or be deposited on the support. The use of support enhances the recovery and reusability of $AuNPs$, for instance after catalysis. The same applies to other methods involving "classic" reducing agents, such as $NaBH_4$. On the other hand, adding different capping agents during the synthesis leads to the preparation of AuNPs with non-spherical shapes, ranging from rods and stars to urchins and more (**J. Li et al., 2011; J. Liu et al., 2017**).

Polysaccharides are biocompatible, biodegradable, non-toxic, and renewable materials that can be conveniently used for one-pot synthesis of AuNPs, eliminating the need for hazardous solvents and reducing/ capping agents (Mizrahy & Peer, 2012). Polysaccharides possess alde□hyde/hemiacetal end groups capable of reducing gold salts, along with numerous other functional groups, such as hydroxyl, amine, and carboxyl groups, which can effectively stabilize forming AuNPs. The inherent biological properties of polysaccharides offer various advan□tages for AuNPs, particularly in biomedicine and theranostics (**Archana et al., 2023; Rajeshkumar et al., 2021; Swierczewska et al., 2016; Yuan, Liu, et al., 2023**). Additionally, certain polysaccharides can serve as a support for the preparation of AuNPs composites due to their natural tendency to form fibers (**He et al., 2020**).

However, methods involving the preparation of $AuNPs$ using natural polysaccharides suffer from several drawbacks (**Chakravarthi et al., 2007; Wang et al., 2017**). These drawbacks mainly arise from the following factors: i) The relatively low density of reducing end-groups, as there is only a single reducing end per polysaccharide macromolecule. ii) The variable amount of reducing end-groups per unit of polysaccharide mass, caused by a naturally wide distribution of molecular weights and the associated high polydispersity. iii) The source-dependent composition and structure of polysaccharides, leading to a variable density of stabilizing groups. These factors pose limitations on the reproducibility and effectiveness of polysaccharide-based AuNPs synthesis, as well as the ability to control their properties.

As an alternative approach, various polysaccharide derivatives have been synthesized and evaluated for the synthesis and stabilization of $AuNPs$. Of particular interest are polysaccharides that have been regioselectively oxidized by periodate ($NaIO_4$) (**Kim et al., 2004; Spedding, 1960**). Their carbonyl groups can directly reduce gold salts while being oxidized to carboxylates. The amount of reducing groups is thus highly increased compared to native polysaccharides, can be controlled by changing the degree of oxidation, and is no longer dependent on the molecular weight of the source polysaccharide. Besides, the formed -COOH groups feature significantly stronger interaction energy with the gold than -OH and $-NH_2$ groups (~40 kcal/mol vs. 10-12 kcal/mol) (**Schmidbaur et al., 2014; Straka et al., 2019**), resulting in better stabilization of $AuNPs$. This modification thus effectively counters major issues of native polysaccharides in $AuNPs$ preparation.

When cellulose is oxidized by periodate, hydroxyl groups in positions 2 and 3 of the anhydroglucose are converted to a pair of reactive -CHO groups, while the macromolecular backbone of cellulose remains largely intact (**Kim et al., 2000; Muchová et al., 2022; Münster et al., 2017**). The degree of oxidation (DO) of resulting 2,3-dialdehyde cellulose (DAC) can be easily controlled by changing the amount of periodate, allowing the preparation of DAC in various forms. For instance, DAC nanocrystals with a relatively high DO of 54 % were utilized by Xiao et al. to synthesize $AuNPs$ with high catalytic efficacy, albeit in the form of a colloid without support (**Xiao et al., 2020**). Zhang et al.

employed cellulose nanofibers with a DO of approximately 30 % to prepare gold and palladium nanoparticles, which exhibited good catalytic efficacy (**Zhang et al., 2018**). However, the resulting particles were larger and the yield was lower compared to the findings reported by Xiao et al. (**Xiao et al., 2020**). On the other hand, the use of bulk support allowed easier and more effective recovery of the composite after the catalysis. The decisive role of DO in $AuNPs$ synthesis has also been confirmed by us for the related 2,3-dicarboxy cellulose (DCC) prepared by secondary oxidation of DAC using chlorite (**Vávrová et al., 2022**). $AuNPs$ prepared using fully oxidized DCC had lower diameters and higher catalytic activity than those prepared using only partially oxidized DCC. In other words, while highly oxidized polysaccharides can be used to prepare $AuNPs$ with higher catalytic activity, their higher solubility results in the absence of bulk support for the formed nanoparticles.

In addition to the one-step methods for preparing $AuNP$ composites, various approaches can be used for the deposition of pre-made and optimized AuNPs. These approaches include spin coating (**F.-K. Liu et al., 2003**), evaporation (**Regiel-Futyra et al., 2015**), electrochemical methods (**Du et al., 2007; Gomathi et al., 2011**), or dip coating (**Cheng et al., 2017; Fahim et al., 2012**). However, the adsorption efficacy of these methods is often limited, leading to the unnecessary losses of expensive $AuNPs$. Moreover, the deposited $AuNPs$ are generally attached to the surface only by weak interactions, which could result in $AuNPs$ leaching.

Here, we introduce a novel and efficient approach for the covalent anchoring of $AuNPs$ onto chitosan nanofibers. In essence, highly catalytically active sub-10 nm $AuNPs$ are prepared by rapid reduction using fully oxidized and solubilized DAC ($AuDAC$). Unlike previously published works, we subsequently utilize the affinity of the reactive carbonyl shell of $AuDAC$ for covalent binding to the amine groups of chitosan nanofibers ($CHIT$). The formed imine bonds are then reduced to more stable secondary amines. This leads to nearly quantitative particle deposition, maximizes the surface coverage of nanofibers, and enhances the pH stability of the final $AuCHIT$ composite, providing a significant improvement over classic dip coating methods. The whole process is schematically depicted in **Scheme 1**. The catalytic activity and reusability of the $AuCHIT$ composite are demonstrated in the reduction of 4-nitrophenol (4-NP) to 4-aminophenol (4-AP) using a custom-built cat-alytical device.

The following hypotheses outline the scope of this study: The fully oxidized DAC enables sub-10 nm $AuNPs$ synthesis; the resulting $AuDAC$s' -CHO-rich shell can form Schiff base with chitosans' -NH_2 groups; the resulting $AuCHIT$ can serve as a reusable catalyst.

2. Materials and methods

2.1. Materials

Cellulose SigmaCell type 20 (weight-average molecular weight $M_w = 76$ kDa, dispersity $Đ = 4.7$, degree of polymerization $DP = 468$, Sigma Aldrich Co.), medium molecular weight chitosan (75-85 % deacety-lated, viscosity-average molecular weight $M_v = 190$-310 kDa, Sigma Aldrich Co.), polyethylene oxide (PEO; $M_v = 600$ kDa, Sigma Aldrich Co.), sodium periodate ($NaIO_4$; VWR, Czech Republic), ethylene glycol (Et-Gly; Penta, Czech Republic), sodium chlorite ($NaClO_2$; 80 % RT, Sigma Aldrich Co.), acetic acid (CH_3COOH; Sigma Aldrich Co.), sodium nitrate ($NaNO_3$; Lachner, Czech Republic) and disodium phosphate dodecahydrate ($Na_2HPO_4 \cdot 12H_2O$; VWR, Czech Republic), gold(III) chloride trihydrate ($HAuCl_4 \cdot 3H_2O$; Sigma Aldrich Co.), sodium hydroxide (NaOH; Lachner, Czech Republic), sodium triacetoxyborohy-dride (STAB; Sigma Aldrich Co.), sodium borohydride ($NaBH_4$; Sigma Aldrich Co.), 4-nitrophenol (4-NP; Sigma Aldrich Co.). All used chemicals were of analytical purity (p.a.) and

used as received without further purification. Demineralized water (conductivity below 0.1 |iS/cm) was used throughout the experiments.

2.2. Preparation of DAC, AuNPs and AuDAC-decorated chitosan nanofibers

2.2.1. Synthesis of DAC

DAC with high DO was prepared by oxidation of cellulose using a 1.2 M excess of $NaIO_4$ at 30 °C for 72 h following earlier works (**Muchová et al., 2022; Münster, Capáková, et al., 2019; Vávrová et al., 2022**). The reaction was terminated by adding ethylene glycol and the resulting DAC was purified by 5 cycles of centrifugation (9000 RPM for 15 min, Thermo Fisher Scientific Sorvall LYNX 4000 centrifuge), and mechanical homogenization (1000 RPM for 10 min, Witeg WiseTis HG-15D ho-mogenizer). Subsequently, the DAC suspension (approx. 0.05 g/mL) was solubilized at 80 °C under reflux for 2 h (**Kim et al., 2004**). Insoluble residues were removed by centrifugation and filtration (0.45 im filter), and the solution was dialyzed using a 14 kDa molecular weight cut-off ($MWCO$) membrane for 24 h and lyophilized. For molecular weight and NMR analysis, DAC was converted to the sodium salt of 2,3-dicar-boxy cellulose (DCC) through chlorite oxidation (**Münster, Fojtů, et al., 2019**). Briefly, the DAC was oxidized for 24 h using $NaClO_2$ (final concentration 0.1 mol/L, 4 x molar excess relative to -CHO groups of DAC; fully oxidized DAC contains 12.5 mmol/g -CHO groups) in the presence of 0.5 mol/L of CH_3COOH. The reaction was terminated by adjusting the pH to 8.5 using NaOH solution, and then the solution was dialyzed using a 14 kDa $MWCO$ membrane for 48 h. The pH was finally adjusted to 7.4 using diluted NaOH solution. The product was filtered using a 0.45 im filter, followed by lyophilization, and stored for further analysis.

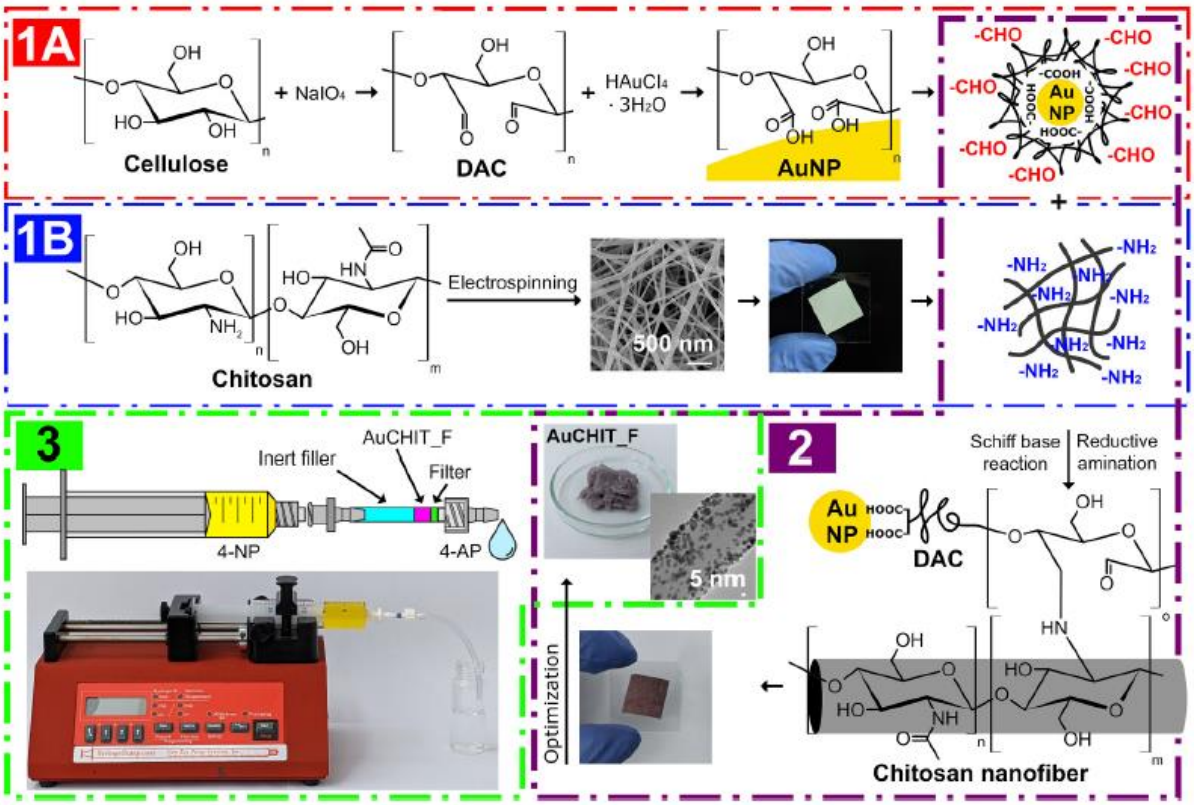

Scheme 1. Overview of experimental effort. 1A) periodate oxidation of cellulose to 2,3-dialdehyde cellulose (DAC), reduction of Au111 salts, and formation of sub-10 nm $AuDAC$ particles; 1B) electrospinning of chitosan solution and preparation of nanofiber chitosan mesh; 2) affinity anchoring of the formed $AuDAC$ on chitosan nanofibers via Schiff base

reaction followed by reductive amination and preparation of highly decorated chitosan nanofiber composite (AuCHIT_F) and 3) the schematics of the catalytic device for 4-nitrophenol (4-NP) catalytic reduction to 4-aminophenol (4-AP).

2.2.2. Synthesis of AuNPs

Initially, optimization of AuNP synthesis using DAC (a screening study) was performed. It focused on varying three main parameters: Series A - weight concentration of DAC (0.1-0.8 wt%), Series B - concentration of $AuDAC$ precursor $HAuCl_4 \cdot 3H_2O$ (0.05-2 mg/mL), and Series C - concentration of NaOH (0-500 pg/mL), see **Table 1**. The following general procedure was used: DAC was dissolved in 5 mL of H_2O using an incubated orbital shaker (VWR, Czech Republic) overnight at 40 °C and the pH was set to 7.0 using diluted NaOH solution.

Table 1 Reaction conditions and sample designation in $AuDAC$ synthesis with variables studied in each series highlighted in bold - weight concentration of DAC (Series A), the concentration of $HAuCl_4 \cdot 3H_2O$ (Series B), and concentration of NaOH (Series C).

		Reaction mixture composition			
		Code	DAC (wt%)	$HAuCl_4 \cdot 3H_2O$ (mg/mL)	NaOH (μg/mL)
Variable synthesis parameter	Series A DAC	$AuDAC_{0.1}$	0.1	0.5	200
		$AuDAC_{0.2}$	0.2	0.5	200
		$AuDAC_{0.4}$	0.4	0.5	200
		$AuDAC_{0.6}$	0.6	0.5	200
		$AuDAC_{0.8}$	0.8	0.5	200
	Series B $HAuCl_4 \cdot 3H_2O$	$Au_{0.05}$ DAC	0.6	0.05	200
		$Au_{0.25}$ DAC	0.6	0.25	200
		$Au_{0.5}$ DAC	0.6	0.5	200
		Au_1 DAC	0.6	1	200
		Au_2 DAC	0.6	2	200
	Series C NaOH	AuDAC_0	0.6	0.5	0
		AuDAC_2	0.6	0.5	2
		AuDAC_20	0.6	0.5	20
		AuDAC_100	0.6	0.5	100
		AuDAC_200	0.6	0.5	200
		AuDAC_500	0.6	0.5	500

Subsequently, 4.7 mL of this solution was transferred into a reaction vial and heated to 90 °C for 15 min. Immediately after heating, a given volume of $HAuCl_4 \cdot 3H_2O$ solution (50 mg/mL) was added to the hot DAC solution and vortexed. Finally, 250 pL of NaOH solution of the given concentration was added to the reaction mixture, initiating the rapid formation of $AuDAC$. The prepared $AuDAC$ solutions were immediately cooled in the freezer and analyzed using the methods listed below.

The main optimization criteria for the screening study were as follows: achieving a low local surface plasmon resonance ($LSPR$) absorbance wavelength, obtaining a high LSPR absorption peak intensity, achieving a high absolute value of the ζ-potential, obtaining a small hydrodynamic radius, and achieving a uniform size distribution. Based on these criteria, the "optimized $AuDAC$ sample" was prepared. Before affinity anchoring onto chitosan nanofibers, the optimized $AuDAC$ sample was

dialyzed against a diluted HCl solution with a pH of 3.5 for 2 h using 1 kDa MWCO membrane to remove residual gold salts, resulting in "production $AuDAC$ sample".

2.2.3. Preparation of chitosan nanofibers

Chitosan ($CHIT$), a linear polysaccharide with N-acetyl-glucosamine and N-glucosamine units linked by β-(1-4) glycosidic bonds, was selected as the substrate for affinity anchoring of $AuDAC$. $CHIT$ features a high density of -NH_2 groups (4.7 mmol/g), can be prepared in the form of nanofibers with a large surface area, and is sufficiently stable to serve as a support for catalytically active $AuNPs$ (**Qiu et al., 2014**). CHIT nanofibers were prepared by dissolving chitosan in 70 % acetic acid at a concentration of 20 mg/mL for 72 h at room temperature. Then, PEO was added as a fiber-forming additive at a weight ratio 5:1 (chitosan: PEO) and stirred for an additional 24 h. The homogeneous mixture had a dynamic viscosity of 1.65 Pa.s and a conductivity of 869 μS/cm. The mixture was filtered using a 1 μm glass filter, degassed, and fed into 8 nozzle jets of SpinLine 40 device (SPUR a.s., Czech Republic) at a rate of 0.15 mL/min. A spinning voltage of 60 kV and a working distance of 21 cm were applied, while maintaining a relative humidity of 25 %. Chitosan nanofibers were electrospun onto a polypropylene (PP) substrate, and each electrospinning cycle lasted for 60 min. The PP substrate, containing spun chitosan nanofibers, was then cut into 3 × 3 cm square specimens, each containing 10 $\pm$ 2 mg of $CHIT$ nanofibers.

2.2.4. Preparation of AuDAC and CHIT (AuCHIT) composite

Initially, samples of 2.5 mg of $CHIT$ nanofibers were immersed in 2.5 mL of the production $AuDAC$ sample solution with pH set to 7 for a specified period (1-168 h), resulting in a set of samples denoted as $AuCHIT$_1-168. After the designated time, the $AuCHIT$ samples were removed from the loading media, thoroughly washed in demineralized water, and placed in a solution of $STAB$ (twice the molar excess relative to -CHO groups of DAC) to reduce the imine bonds to secondary amines. The samples were then washed again in demineralized water, and lyophilized. The UV-Vis absorbance intensity of the production $AuDAC$ sample solution was measured before and after the loading procedure to determine the $AuDAC$ anchoring efficacy. Next, the final (bulk) sample AuCHIT_F was prepared by mechanically homogenizing 100 mg of chitosan nanofibers in 100 mL of $AuDAC$ solution for 40 min at 1000 RPM using a mechanical homogenizer, followed by shaking for 2 h and 20 min (i.e., a total AuNPs loading time of 3 h). The AuCHIT_F suspension was thoroughly washed on a filter with demineralized water, redispersed using a mechanical homogenizer, reduced by $STAB$, washed again on a filter, and lyophilized. The lyophilized AuCHIT_F sample was then characterized (as described in **Section 2.5**) and used as the active component in the catalytic device (see **Section 2.6**).

2.2.5. Test of affinity anchoring proces

The $CHIT$ nanofibers were soaked in two different solutions: a) pure 0.6 wt% DAC solution to study the imine formation, and b) the production $AuDAC$ sample for 3 h before treatment with $STAB$ to study the formation of secondary amines and the anchoring of nanoparticles. The washed and dried samples, along with the source $CHIT$ and DAC, were analyzed using $FT-IR$.

2.3. Characterization of DAC

2.3.1. Infrared spectroscopy (FT-IR)

The qualitative spectral analysis of the prepared DAC was performed using an $FT-IR$ spectrometer Nicolet 6700 (Thermo Fisher Scientific, USA) equipped with a diamond crystal and operated in ATR mode. The spectral analysis covered the wavenumber range from 4000 to 600 cm^{-1}.

2.3.2. Gel permeation chromatography (GPC)

GPC analysis was carried out on DCC, following the method reported earlier (**Münster et al., 2017**). The analysis employed a Waters $HPLC$ Breeze chromatographic system (Waters, USA), equipped with a refractive index detector Waters 2414 (drift tube $T = 60$ °C) and a Tosoh TSK gel $GMPW_{xl}$ column (300 mm × 7.8 mm × 13 μm, column $T = 30$ °C). The mobile phase consisted of a mixture of 0.1 M $NaNO_3$ and 0.05 M $Na_2HPO_4 \cdot 12H_2O$. Pullulan polysaccharide calibration kit SAC-10 (M_w = 342-805,000 g/mol, Agilent Technologies, USA) was used.

2.3.3. Nuclear magnetic resonance (NMR)

To accurately quantify the DO of the prepared DAC, ^1H, and ^{1}H—^{13}C correlation spectra of the DCC derivative were recorded using a JEOL 400 MHz NMR spectrometer (JEOL, Japan). The measurements were performed at $T = 298$ K in D_2O. The DO was determined by comparing the integral intensities of the H4 and H5 signals around 4 ppm with the signals of non-oxidized cellulose, which are typically found between 3.0 and 3.5 ppm according to previous works (**Münster et al., 2021, 2020**).

2.4. Characterization of AuDAC

2.4.1. Ultraviolet—visible spectroscopy (UV-Vis)

The $LSPR$ values of $AuDAC$ diluted solutions were measured by a double-beam $UV-Vis$ spectrometer Lambda 1050 (PerkinElmer, USA) in the range of wavelength from 250 to 800 nm.

2.4.2. Transmission electron microscopy (TEM)

JEM-2100 transmission electron microscope (JEOL, Japan) operated at an acceleration voltage of 160 keV was employed for sample imaging. Diluted $AuDAC$ solutions were drop-cast onto a 300 mesh copper grid coated with a Formvar membrane and gently dried.

2.4.3. Dynamic light scattering (DLS)

Hydrodynamic radius (r_h) and Zeta potential (ζ) of $AuDAC$ diluted solutions were measured by a Zetasizer Nano ZS90 instrument (Malvern Instruments, UK). The temperature was set at 25 °C on a DTS1070 cell using the Smoluchowski model.

2.4.4. X-ray fluorescence (XRF)

The concentration of Au in the optimized and production $AuDAC$ samples was determined using an energy-dispersive X-ray fluorescence spectrometer by ARL Quant'X EDXRF Analyzer (Thermo Fisher Scientific, USA). Calibration standards were prepared by dissolving a defined amount of $HAuCl_4 \cdot 3H_2O$ solution in water.

2.5. Characterization of AuCHIT

Besides methods described in Section 2.4, $AuCHIT$ samples were also analyzed by:

2.5.1. Scanning electron microscopy (SEM)

Images of chitosan nanofibers and $AuCHIT$ samples were obtained using a Nova NanoSEM 450 microscope (FEI, Czech Republic) operated at a 5 kV accelerating voltage. The samples were sputtered with gold-palladium nanoparticles to suppress the charge accumulation effect.

2.5.2. Diffuse reflectance integration sphere UV-Vis spectral analysis (DUV-Vis)

The $DRUV - Vis$ measurements of the composite sample in the ambient atmosphere were conducted using a UV-Vis spectrometer Perkin-Elmer Lambda 1050 with a 150 mm integration sphere.

2.5.3. Inductively coupled plasma optical emission spectrometry (ICP-OES)

The content of Au in the prepared composites was determined by $ICP - OES$ spectroscopy performed on an iCAP 6500 spectrometer (Thermo Fisher Scientific, USA) utilizing Au spectral lines at 242.795 and 267.595 nm.

2.5.4. Specific surface area analysis (BET)

Chitosan nanofibers and final bulk AuCHIT_F sample were degassed at 70 ° C for 48 h. The specific surface area (as BET) was determined by a multipoint Brunauer-Emmet-Teller (BET) analysis. The adsorption and desorption isotherms were recorded at 77 K using a high-precision surface area analyzer Belsorp-mini II (BEL Japan Inc., Japan).

2.5.5. Stability study

A final bulk AuCHIT_F sample was placed in PBS solutions (0.4 mg of AuCHIT_F per mL of PBS) of different pH (3, 7 and 9). After 24 h exposure, dialysis was performed for 24 h using 10 kDa MWCO membrane against 5 L water. The samples were then lyophilized and imaged using SEM and TEM.

2.6. AuDAC catalytic efficacy and AuCHIT catalytic device assembly and catalysis

2.6.1. Evaluation of AuDAC catalytic efficacy

The catalytic efficacy of the optimized $AuDAC$ sample was evaluated by employing a previously established approach (**Vávrová et al., 2022**). The catalytic reduction of 4-NP to 4-AP was performed in

the presence of NaBH4 under the following conditions: 1 mL of NaBH4 (7.5 mg/mL) was diluted with 1.7 mL of demineralized H_2O, and 0.1 mL of 4-NP (0.71 mg/mL) was added. To initiate the catalytic reaction, 0.2 mL of $AuDAC$ solution (0.01 and 0.001 mg/mL of AuNPs) was added. The catalytic mixture (c_{4-NP} = 0.17 mmol/L, c_{NaBH4} = 66 mmol/L) was measured using a Lambda 1050 $UV-Vis$ spectrometer (PerkinElmer, USA) at 25 °C, acquiring spectra in (i) the range from 350 to 450 nm at given time intervals (1-7 min), and in (ii) time-sweep mode at 400 nm to observe the decrease in 4-NP absorbance over time (t) until constant absorbance readings were obtained. A blank experiment was performed without $AuDAC$ but with an equivalent amount of DAC, to investigate potential side reactions with the substrate. The absorbance of the AuNPs at around 400 nm was neglected due to the low concentration of $AuDAC$. The catalytic reduction follows pseudo-first-order kinetics, allowing the determination of the rate constant (k) as the slope of $\ln(c_t/c_0)$ plotted against t. The turnover frequency (TOF) of the prepared $AuDAC$, corresponding to moles of reactant converted by a given amount of catalyst per minute, was determined according to (**Kozuch & Martin, 2012**) and expressed for the initial concentration of 4-NP.

2.6.2. Evaluation of AuCHIT catalytic efficacy

To evaluate the catalytic efficacy of composites, the catalytic device depicted in Scheme 1 was constructed. It consisted of a male Luer-lock adapter connected to a 2.5 cm long PP tubing with a 3 mm inner diameter, which was then connected to a female Luer-lock adapter. The PP tubing was sealed using type 474 filter paper (VWR, Czech Republic) and filled with a mixture of 2 mg of $AuCHIT\_F$ (containing 0.209 mg of $AuDAC$) and 10 mg of cotton wool, which was prepared by stirring both components in water for 1 h. The active catalytic layer had a length of approx. 2 mm and it was overlaid with an additional 10 mg of cotton wool filler (approx. 6 mm in length) to prevent movement and contact with a filter paper at the end of the PP tubing. The catalytic device was connected to a 20 mL Luer-lock syringe filled with 6 mL of a catalytic medium described above. The setup was mounted in a NE-1000 one-channel programmable syringe pump (New Era Pump Systems Inc., USA), and the flow rate was set to 0.25, 0.5 and 0.75 mL/min. In a typical experiment, 1 mL of catalytic medium was discarded before sampling to fill the dead volume of the device and ensure proper wetting. The sampled volume of 4 mL was then analyzed using a Lambda 1050 $UV-Vis$ spectrometer (PerkinElmer, USA) in the wavelength range from 250 to 800 nm. After sampling, the catalytic device was washed with 10 mL of water at a flow rate of 0.5 mL/min. The experiments were repeated 3 × for each employed flow rate to investigate reproducibility.

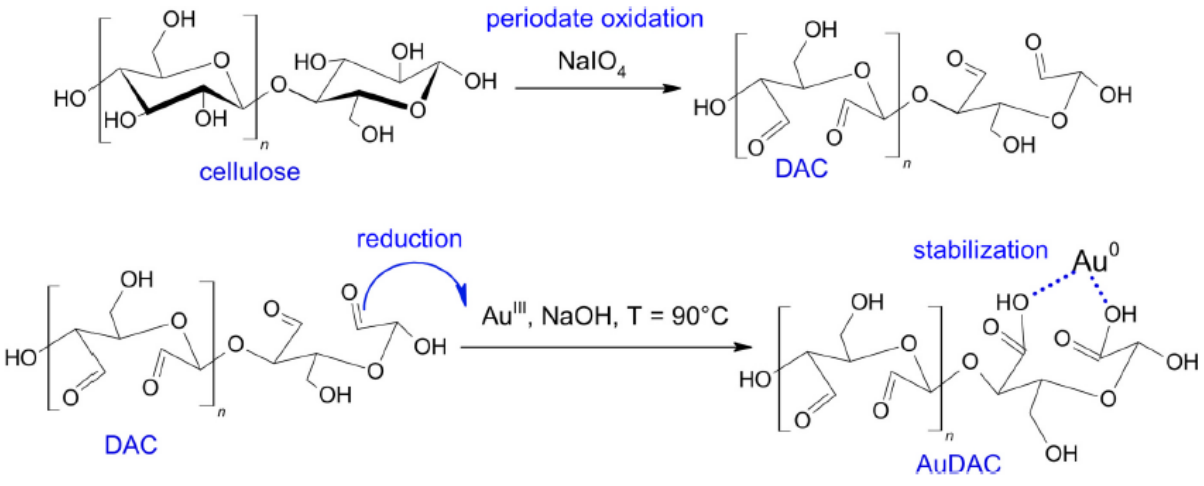

Scheme 2. Oxidation of DAC (top row) and the mechanism of Aum reduction and stabilization via DAC (bottom row).

3. Results and discussion

3.1. DAC characterization and AuNPs screening study

The oxidation of cellulose by periodate results in the formation of a pair of highly reactive carbonyl (-CHO) groups, as depicted in **Scheme 2** (top row). The IR spectrum of DAC can be found in Fig. S1 in the Supplementary Information (SI). In addition to the usual absorption peaks of cellulose, the DAC IR spectrum exhibits a characteristic $C = O$ absorption band at 1730 cm^{-1} from the introduced aldehyde groups. Due to the tendency of DAC to form various hemiacetals, as evidenced by an increase in the intensity of the $C - O - C$ vibration band at 885 cm^{-1} (**Münster et al., 2017**), DAC was converted to DCC by chlorite oxidation before GPC analysis to obtain a more reliable measurement of its molecular weight distribution (**Münster, Fojtů, et al., 2019**). The M_w of DCC was determined to be 14 kDa ($Đ = 1.65$). The solubilized DAC macromolecules are thus comprised of approx. 50 monomer units.

NMR spectra of DCC were used to determine the DO, as $DO_{DAC} = DO_{DCC}$ (**Münster et al., 2020**). ^{1}H NMR and $^{1}H - ^{13}C$ correlation NMR spectra of DCC can be found in Fig. S2 in the SI. Oxidation was found to be nearly quantitative ($DO = 99$ %). NMR spectra of DAC are unsuitable for this purpose due to the structural complexity of DAC's inter-/intra-molecular hemiacetals formed after oxidation. For comprehensive NMR analysis of DAC structure in solution, identification of various hemi-acetals, and signal assignment, see our previous work (**Münster et al., 2017**).

DAC was subsequently utilized as a reducing and stabilizing agent for the preparation of $AuDAC$, as illustrated in the bottom row of **Scheme 2**. During the reduction of Au^{III} salt, the $-CHO$ groups of DAC undergo oxidation, resulting in the formation of a pair of carboxyl ($-COOH$) groups. These $-COOH$ groups electrostatically stabilize the developing $AuDAC$ seeds. To obtain $AuDAC$ particles with the sub-10 nm dimensions (presumably exhibiting the highest catalytic activity) and high stability, three variables were screened: the weight concentration of DAC, the concentration of $HAuCl_4 \cdot 3H_2O$, and the concentration of NaOH, see **Fig. 1**.

In Series A, the $LSPR$ wavelength of $AuDAC$ remains around 525 nm and is largely unaffected by the varying weight concentration of DAC, indicating the formation of relatively small $AuDAC$ in all cases. The comparable intensity of the $LSPR$ band across $AuDAC$ samples prepared using 0.2-0.8 wt% DAC suggests similar synthesis yields. In contrast, using 0.1 wt% DAC results in the formation of only a very small amount of $AuDAC$.

The stability of nanoparticles, expressed by ζ-potential, was more or less similar (below — 30 mV) for the whole of Series A, indicating good stability of formed $AuDAC$. The smallest nanoparticles were obtained for $AuDAC_{0.6}$ (r_h around 24 nm according to DLS, i.e., including ionic/polymeric corona; size distribution of 6.4 ± 1.2 nm according to TEM, see the top right part of **Fig. 1**).

The weight concentration of DAC was thus fixed at 0.6 wt% in Series B (middle row of **Fig. 1**), and the concentration of the $HAuCl_4 \cdot 3H_2O$ was varied. The $UV - Vis$ analysis reveals that increasing the precursor concentration leads to an increase in the LSPR absorbance wavelength from 517 to 544 nm. However, the $LSPR$ absorbance intensities exhibit a distinctly A-shaped trend, with the maximum intensity observed for $Au_{0.5}$DAC. The $Au_{0.5}$DAC also exhibits the smallest particles, having rh of approx. 20 nm according to DLS, and a relatively narrow size distribution of 5.7 ± 1.1 nm according to TEM.

Therefore, $HAuCl_4 \cdot 3H_2O$ concentration was set to 0.5 mg/mL in the subsequent series C, where the concentration of NaOH was varied.

The concentration of NaOH plays a crucial role in initiating the nanoparticle growth phase. Low NaOH concentrations (0, 5, and 20 μg/ mL) are insufficient to initiate significant $AuNP$ growth, resulting in $LSPR$ bands of very weak intensity. Conversely, the highest NaOH concentration (500 μg/mL) leads to the formation of an intensive $LSPR$ band but with a wavelength of 542 nm, and thus to the formation of very large $AuNPs$. Such a high NaOH concentration may also cause degradation of DAC via the β-elimination mechanism, making it unsuitable for the $AuDAC$ preparation. The best results were obtained using 200 μg/mL NaOH ($AuDAC\_200$), resulting in nanoparticles with r_h = 25 nm (~5 nm according to TEM) and a narrow size distribution. It is worth noting that the preparation conditions for $AuDAC\_200$ are identical to those of $Au_{0.5}$DAC and $AuDAC_{0.6}$, yielding very similar results. Thus, the reproducibility of $AuDAC$ synthesis is high.

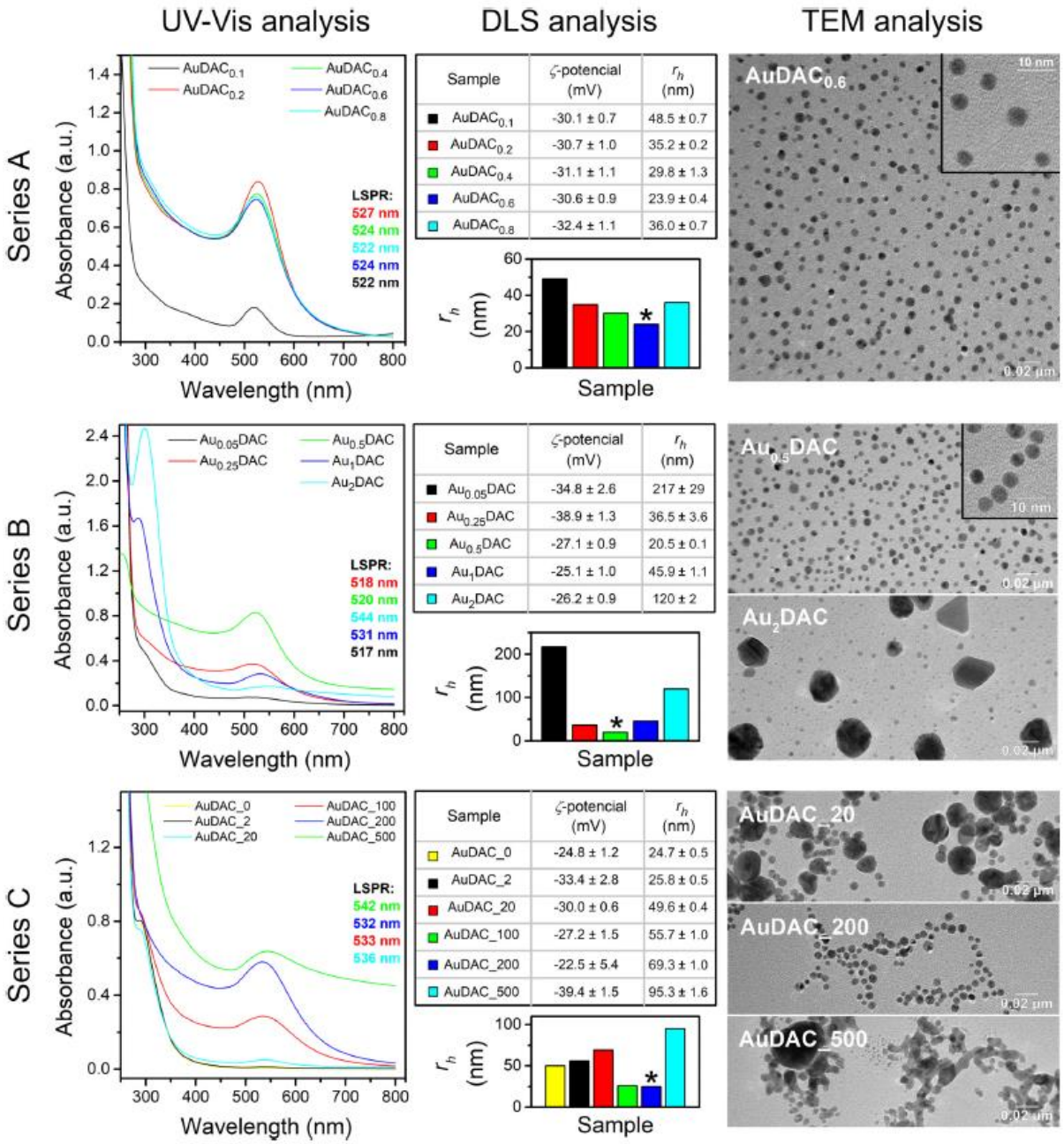

Fig. 1. The $UV-Vis$ ($LSPR$ values) results, DLS (ζ-potential and hydrodynamic radius, r_h), and TEM analyses of the $AuDAC$ preparation screening study. Variation of: Series A - weight concentration of DAC (0.1-0.8 wt%), Series B - concentration of $HAuCl_4 \cdot 3H_2O$ (0.05-2 mg/mL), and Series C - concentration of NaOH (0-500 μg/ mL). Samples are color-coded for easier comparison. Asterisk marks the samples with the smallest r_h.

Next, the stability of the optimized $AuDAC$ sample (0.6 wt%, 0.5 μg/ mL $HAuCl_4 \cdot 3H_2O$, 200 μg/mL NaOH) was examined with and without further purification (for details see **Section 2.2**). In an unpurified sample, the intensity and wavelength of $LSPR$ changed significantly over 96 h due to the slow growth of $AuDAC$ particles in the presence of residual precursor. However, no significant changes were observed in the purified sample, as shown in **Fig. 2**. Therefore, the purified sample can be safely stored before further use. It is important to note that the unreacted DAC was intentionally not removed (using a 1 kDa $MWCO$ dialysis membrane) as it was later used to stabilize the chitosan fibers.

According to XRF analysis, the purified sample contained 0.2088 mg/mL of Au, which corresponds to a high reaction yield of 91 %.

Overall, the ability of DAC to rapidly and efficiently reduce Au^{III} and subsequently stabilize $AuNPs$ was confirmed, and optimal reaction conditions were determined. The rate of $AuDAC$ formation is very fast, occurring instantly after NaOH addition, which is highly advantageous compared to syntheses using natural polysaccharides or dicarboxy polysaccharides, which can take several hours (**Vávrová et al., 2022**). The resulting carbonyl-decorated $AuDAC$ nanoparticles were subsequently used for affinity anchoring onto electrospun chitosan nanofibers.

3.2. AuCHIT preparation and characterization

Given the (i) macromolecular nature of DAC, (ii) high density of highly reactive $-CHO$ groups on the DAC backbone, and (iii) the excess of DAC in the reaction mixture, only a fraction of DACs' $-CHO$ will be oxidized to carboxylates during the $AuDAC$ preparation. The remaining carbonyl groups are located in a shell on the $AuDAC$ surface and spontaneously react with $-NH_2$ groups from chitosan nanofibers upon the formation of Schiff bases (**Scheme 3**A). This process has been labeled as "affinity anchoring" in this work given its nearly quantitative effectivity, vide infra, and was used to prepare the $AuDAC$/chitosan nanofiber ($AuCHIT$) composite. Because imine bonds between $-CHO$ of DAC and $-NH_2$ groups of $CHIT$ are so-called dynamic covalent bonds, i.e. reversible by definition and prone to disruption in the acidic environment, the reduction of imines to stable secondary amines by $STAB$ was performed (**Scheme 3**B) to improve the stability of the $AuCHIT$ composite.

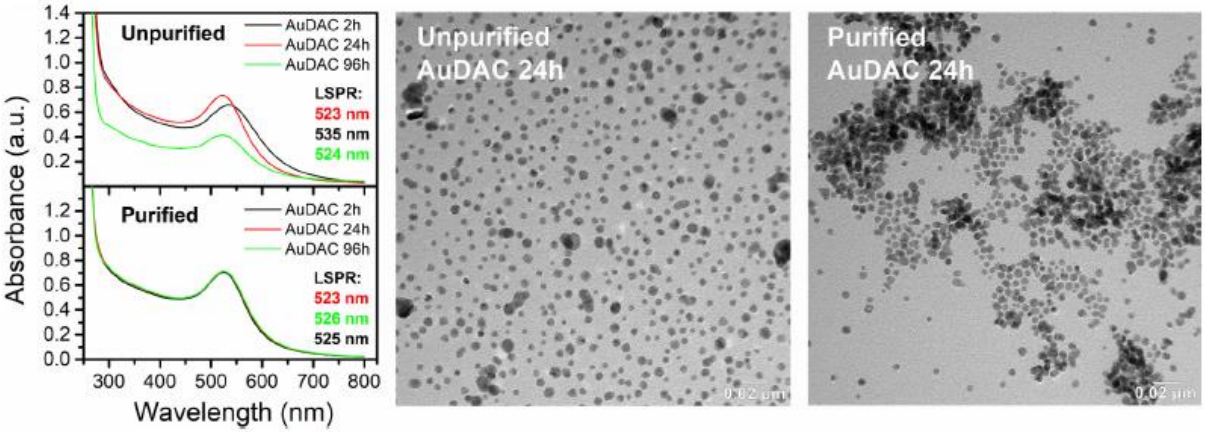

Fig. 2. The influence of purification evaluated by comparison of $UV-Vis$ spectra and TEM micrographs of optimized $AuDAC$ sample (unpurified) and production $AuDAC$ sample (purified).

The affinity anchoring was confirmed by IR analysis, as shown in **Figs. 3** and S3 in SI. While the IR spectrum of pure $CHIT$ shows its typical absorption bands at 1650 cm^{-1} (amide I vibration mode of N-acetyl groups), 1565 cm^{-1} ($N-H$ bending of the primary amine), and $C-O$ stretching vibrations at 1075 and 1030 cm^{-1} (**Fernandes Queiroz et al., 2014**), and IR spectrum of DAC features an aldehyde carbonyl stretching band at 1730 cm^{-1} and $C-O$ stretching vibration at 1025 cm^{-1}, the $N-H$ bending vibration of the primary amine at 1565 cm^{-1} essentially disappears in the $CHIT-DAC$ spectrum in **Fig. 3**, and the intensity of the carbonyl stretching vibration of DAC at 1730 cm^{-1} decreases significantly. This is consistent with the reaction between DACs' $-CHO$ and $-NH_2$ groups of $CHIT$. According to the literature, the vibration of the imine bond itself is relatively weak and should be found around 1630-1640 cm^{-1} (**Heinert & Martell, 1962**). Imine formation between DAC and $CHIT$ is thus likely represented by the appearance of the vibration at 1640 cm~1 in the CHIT-DAC spectrum, which overlaps with existing bands of DAC (1635 cm^{-1}) and chitosan (1650 cm^{-1}). Note, that in the $AuCHIT$ sample, i.e., after treatment by $STAB$, this band disappears, and only the DAC band at 1635 cm^{-1}

remains visible. This is consistent with the reduction of imines to secondary amines. The existence of covalent bonds between $AuDAC$ and $CHIT$ is further supported by the appearance of the secondary amine vibration at 1065 cm^{-1} (compare $CHIT - DAC$ and $AuCHIT$ spectra in **Fig. 3**). Other groups have also reported similar changes in $FT - IR$ spectra during DAC and $CHIT$ coupling (**Gao et al., 2021; Kim et al., 2017**). To summarize, the $FT - IR$ spectra show that both free DAC and $AuDAC$ bind to the $CHIT$ nanofibers.

Next, the affinity anchoring ($AuDAC$ loading) reaction kinetics was studied by SEM, TEM, and $ICP - OES$ analysis after 1, 3, 6, 24, and 168 h at pH 7 ($AuCHIT\_1$ to $AuCHIT\_168$ samples in **Fig. 4**). As can be seen in **Fig. 4** A, the 1 and 24-h-long loading procedures led to a 14 % and 24 % decrease in the $LSPR$ intensity of the loading $AuDAC$ solution, respectively. The DRUV-Vis analysis of $AuCHIT\_1$ and $AuCHIT\_24$ samples using the integration sphere (**Fig. 4**B) showed that both in $LSPR$ bands are at around 530 nm, similar to free $AuDAC$ colloidal solution, indicating that the loading procedure proceeds without particle aggregation. Surprisingly, the residual $LSPR$ intensity of $AuDAC$ significantly increases after 168 h of loading, i.e., the $AuDAC$ deposition is decreased over time. TEM analysis of $AuCHIT$ (**Fig. 4**C and D) reveals the reason behind this phenomenon. While the $AuCHIT\_1$ sample consists of densely $AuNP$s-covered chitosan nanofibers with a smooth surface, the micrograph of the $AuCHIT\_168$ sample shows less densely $AuDAC$-decorated nanofibers with uneven "eroded" surface. A prolonged loading procedure before reduction thus leads to the undesirable flaking of the outer layer of chitosan nanofibers and the formation of $AuCHIT$ clusters in the solution.

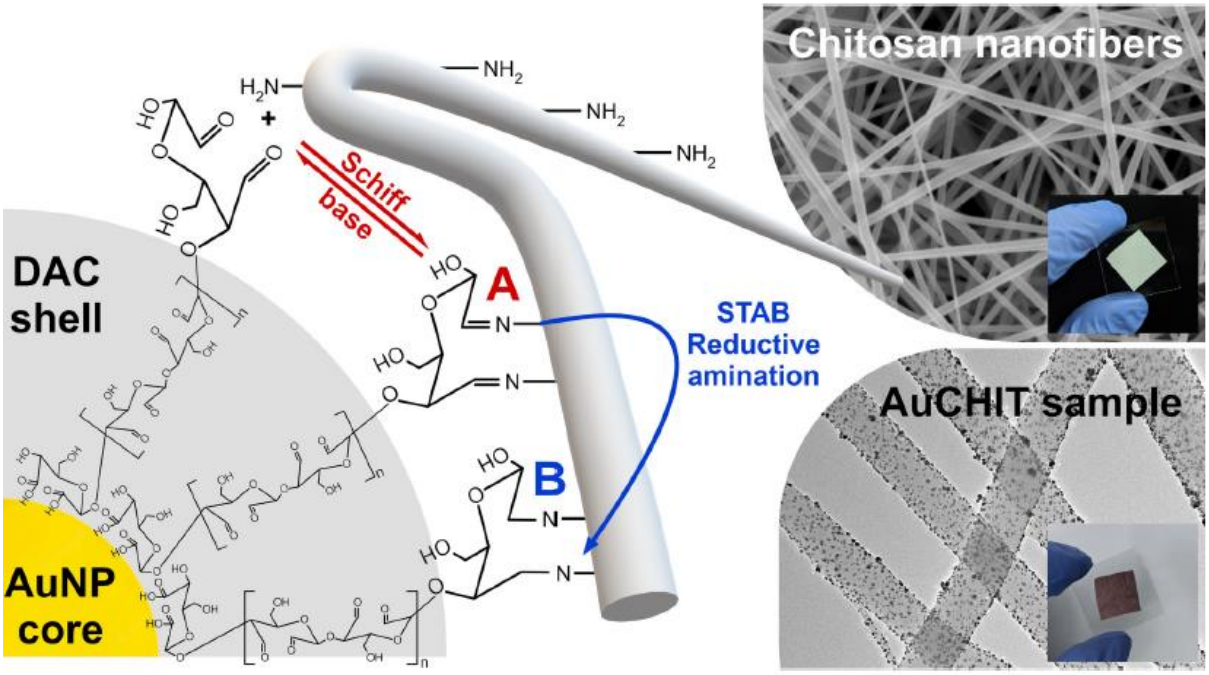

Scheme 3. Shows the $AuNPs$ affinity anchoring via its DAC shell onto -NH2-rich chitosan nanofiber surface utilizing Schiff base reaction and subsequent reduction of imine bond via reductive amination by $STAB$.

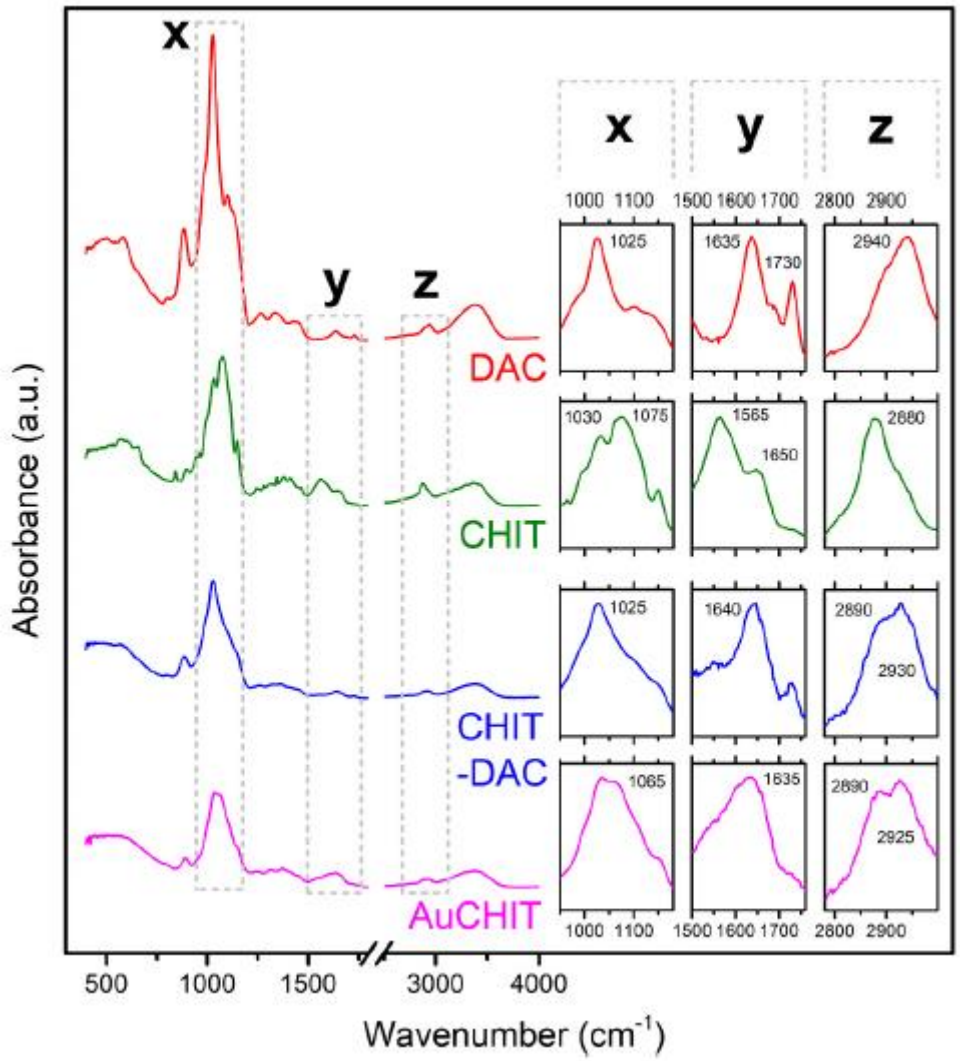

Fig. 3. FT-IR analysis of DAC (red lines), CHIT (green lines), unreduced $CHIT - DAC$ (blue lines) bound by imine bonds, and $AuCHIT$ composite (fuchsia lines) in which $STAB$ reduces imine bonds to amines. For separate full-size IR spectra of each sample see Fig. S3

However, anchoring of $AuNPs$ in this setup is limited to only a few surface layers of chitosan nanofibers, as evident from the loss of reddish color upon scratching the $AuCHIT$ specimen surface in **Fig. 4**E1, and the difference between SEM images of the outer and inner sections (parts E2-E4 in **Fig. 4**). The dense outer layer of chitosan nanofibers likely swells in the solution, preventing $AuDAC$ particles from reaching the inner parts of the specimen. Consequently, the loading efficacy of $AuDAC$ is reduced due to the limited surface area of the substrate. To address this limitation, chitosan nanofiber sheets were mechanically homogenized (see **Section 2.2** for more details), which significantly increased the surface available for $AuNPs$ affinity anchoring and greatly improved the $AuDAC$ loading efficacy. The $LSPR$ absorption band of the loading solution at 524 nm (red line in **Fig. 5**A) completely disappeared after 3 h (black line), and according to XRF analysis, only 1 % of Au remained in the loading medium after 3 h. The quantitative nature of AuDAC anchoring is evident even with the naked eye, as shown in the inset photograph of the loading solution before and after loading in **Fig. 5**A. Note that all reaction conditions remained the same as before, with the only change being the homogenization of the chitosan sample. Additionally, the $ICP - OES$ of the $AuCHIT$_F sample also showed almost a 3 × higher Au content (10.44 wt%) compared to the $AuCHIT$_3 sample (3.72

wt%), which was prepared without mechanical homogenization. The anchoring of $AuDAC$ also resulted in the two-fold increase of the specific surface area of $AuCHIT$_F (see **Fig. 5**B) compared to bare chitosan nanofibers, i.e., $\alpha_s\ BET_{\text{AuCHIT\_F}} = 27.4$ m^2/g versus as bet chitosan $= 14.2$ m^2/g. The macroscopic photograph, SEM, and TEM micrographs of the $AuCHIT$_F sample (**Fig. 5**C) confirmed densely decorated chitosan nanofibers throughout the sample.

Next, the stability of the resulting $AuCHIT$_F composite was investigated. Even after stirring at pH 3 for 24 h, no changes in the structure of the $AuCHIT$_F nanofibers, their erosion, or nanoparticle leaching were visible, although such conditions would normally completely dissolve the $CHIT$ nanofibers. This exceptional stability can be attributed to the crosslinking of nanofiber surface by free DAC left after the $AuDAC$ synthesis, which chemically strengthens the final composite, and to the covalent anchoring of $AuDAC$ nanoparticles.

In summary, the affinity anchoring of $AuDAC$ onto $CHIT$ nanofibers through a Schiff base reaction and subsequent reductive amination offers an almost quantitative level of efficacy, and the resulting composite exhibits remarkable stability across a broad pH range.

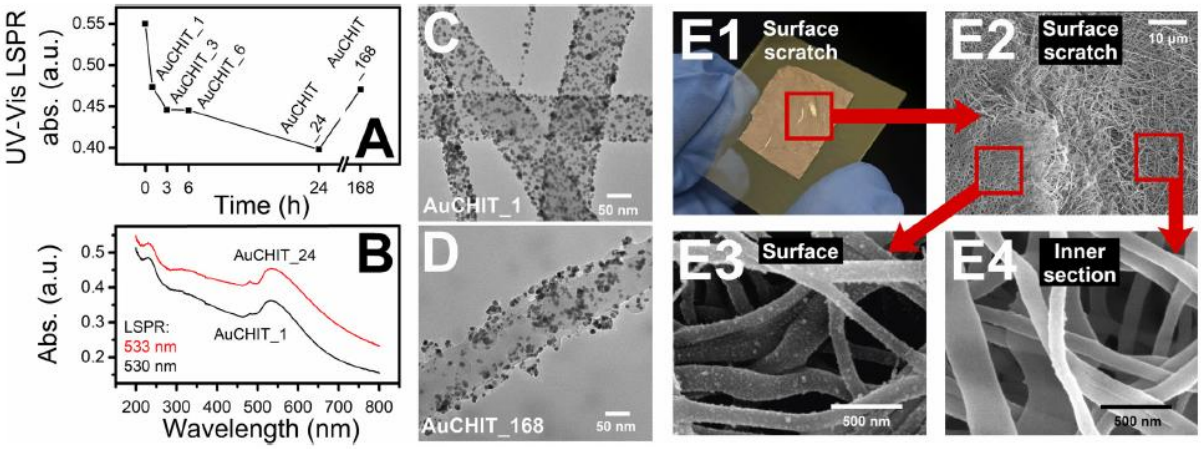

Fig. 4. Part A - The evolution of residual $LSPR\ UV-Vis$ intensity of $AuDAC$ sample as a function of time. Part B - $LSPR$ values for two selected AuCHIT samples ($DRUV-Vis$ analysis); Parts C and D - TEM micrographs of $AuCHIT$_1 and $AuCHIT$_168, respectively, evidencing the loss of $AuNPs$ from chitosan nanofibers' surface in the latter. Part E - Comparison of surface and inner regions of $AuCHIT$, showing the absence of $AuDAC$ inside of the chitosan nanofiber specimens, likely due to steric hindrance of surface chitosan fibers swelled in the solution, demonstrated by scratching the surface of a loaded specimen (part E1), and by SEM micrographs of the surface and inner sections (parts E2-E4).

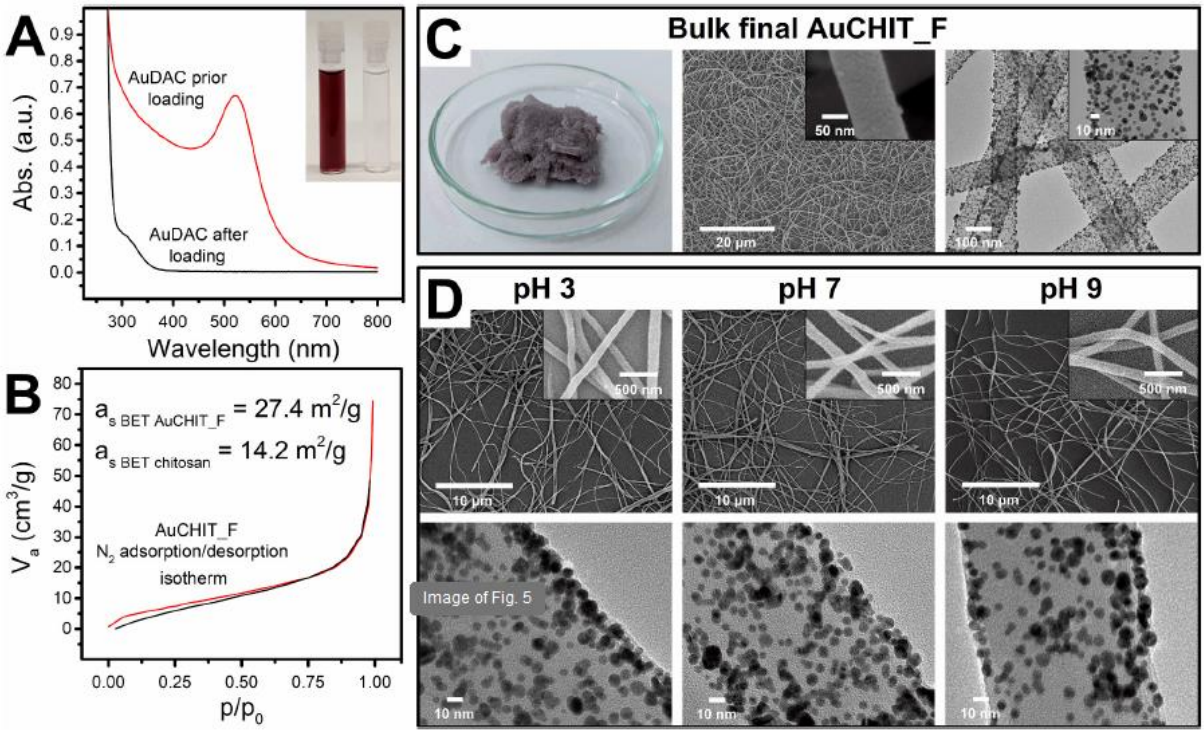

Fig. 5. Summary of the analyses conducted on the $AuCHIT_$F material. Part A shows the $UV-Vis$ spectra of the loading medium ($AuDAC$) before and after the loading and the photograph of the respective solutions. Part B shows the results of BET analysis - the example of N_2 adsorption/desorption isotherm and specific surface area ($a_{s\ BET}$) of $AuCHIT_$F, and $CHIT$ nanofiber samples. Part C shows SEM and TEM micrographs of $AuCHIT_$F and part D exemplifies the pH stability of $AuCHIT\_F$ (24 h, PBS, pH 3-9) using SEM and TEM analysis.

3.3. Catalytic efficacy of AuDAC and AuCHIT device

The catalytic efficacy was evaluated using the model reduction reaction of 4-NP to 4-AP in the presence of borohydride. This approach enables a robust and straightforward determination of catalytic efficacy by observing the decrease of 4-NP absorption intensity at 400 nm using $UV-Vis$ analysis. This catalysis reaction is widely employed, allowing for a direct comparison with previous studies. The reaction follows the Langmuir-Hinshelwood mechanistic model proposed by (**Wunder et al., 2010**). Borohydride ions and 4-NP molecules bind and "re-structuralize" on the $AuNPs$ surface via substrate ligand displacement, resulting in the formation of 4-AP (see **Fig. 6** A).

Initially, the catalytic efficacy of the production $AuDAC$ sample was determined as described in Section 2.6, (see **Fig. 6**C-E). Using 2 pg of $AuDAC$ catalyst, 90 % of 4-NP is converted to 4-AP in approx. 7 min (TOF = 15.9 min^{-1}, k = 0.3 min^{-1}, see **Fig. 6**C and D). This represents a significant increase in catalytic efficacy compared to our previous study focused on the $AuNPs$ prepared using dicarboxy polysaccharide derivatives, i.e., $AuDCC$ (20 μg of $AuDCC$ - conversion t = 2.8 min, TOF = 7.6 min-A k = 1.5 min-A (**Vávrová et al., 2022**). In other words, a 10 × lower amount of $AuDAC$ catalyst exhibits a 2 × higher TOF. When the amount of $AuDAC$ catalyst was reduced to 0.2 μg in the same catalytic system (**Fig. 6** E), TOF increased to 27.1 min^{-1}, while the rate constant k decreased to 0.07 min^{-1}. A comparison with other catalyst systems based on $AuNPs$ can be found in our previous work (**Vávrová et al., 2022**). Prepared $AuDAC$ particles are among the most effective, likely due to their small dimensions.

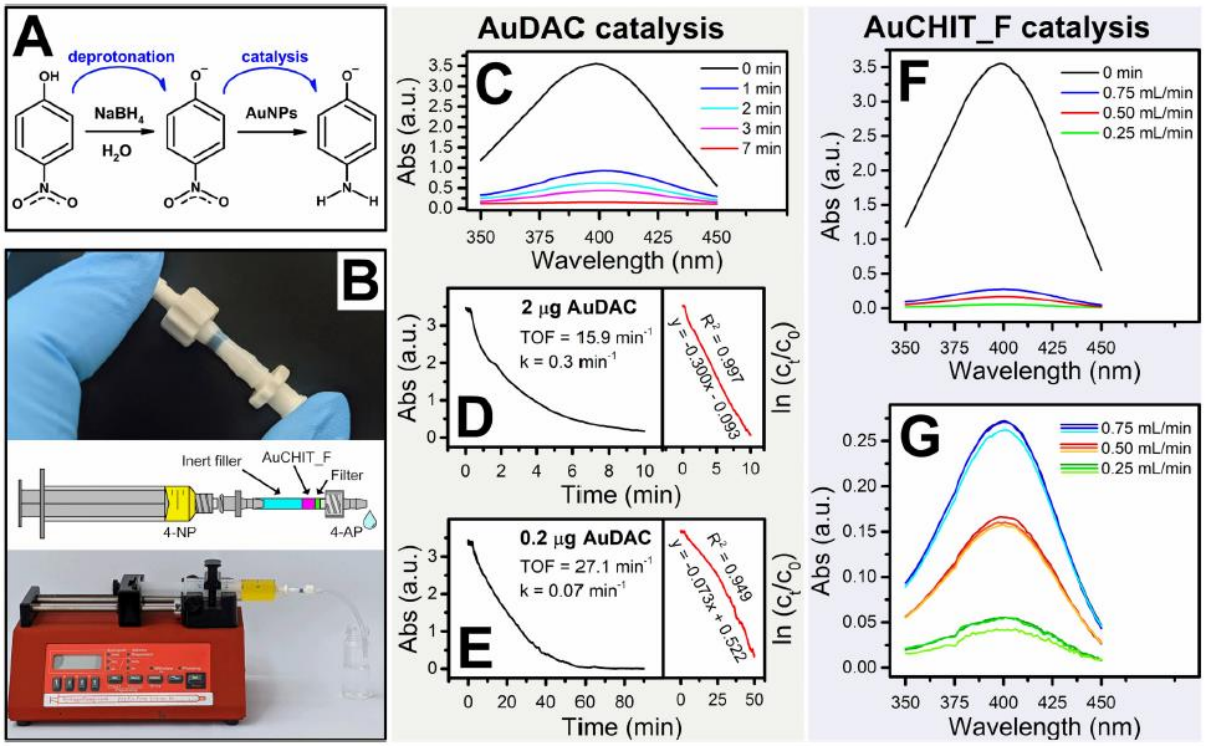

Fig. 6. Summary of catalytic efficacy of $AuDAC$ and catalytic device based on $AuCHIT$_F. Part A shows the reaction scheme of 4-NP to 4-AP conversion. Part B shows the assembly of the catalytic device based on $AuCHIT$_F. Parts C-E summarize the catalytic efficacy of $AuDAC$. Part C shows time-resolved $UV-Vis$ spectra of the catalytic system containing 2 μg of $AuDAC$ in the range from 350 to 450 nm. Time-sweep experiment showing a decrease of intensity of 400 nm band characteristic for the 4-NP reduction for 2 μg (part D) and 0.2 μg (part E) of $AuDAC$ with noted TOF and k values and $\ln(c_t/c_0)$ plots. Parts F and G summarize results on 4-NP to 4-AP catalysis using $AuCHIT$_F. Part F shows the influence of the different flow rate (0.25-0.75 mL/min) on the $UV-Vis$ 4-NP band intensity in the 350-450 nm region. Part G shows the reproducibility of catalysis for each flow rate expressed as the $UV-Vis$ 4-NP band intensity in the 350-450 nm region after each catalytic cycle.

As the catalytic efficacy of $AuCHIT$_F cannot be reliably studied directly in a $UV-Vis$ tube (unsoluble composite could interfere with $UV-Vis$ measurements), a specialized device was constructed, see **Fig. 6**B and **Section 2.6**. This setup also more accurately represents industrial catalytic columns and thus should provide more realistic results. The catalytic efficacy and reproducibility results are shown in **Fig. 6**F and G.

Note that using the employed setup, the flow rate of the medium dictates the catalytic performance. Even at the fastest flow rate of 0.75 mL/min, a 92.4 % reduction of 4-NP to 4-AP was achieved. Unsurprisingly, slower flow rates exhibit even higher conversions (i.e., 0.50 mL/ min - 95.5 %, 0.25 mL/min - 98.6 %). Given the linear dependence of the conversion rate on the flow, the 90 % conversion would be reached at a 1 mL/min flow rate. The TOF value at 0.75 mL/min flow rate is 0.28 min^{-1} (corresponding to 0.36 min^{-1} at 1 mL/min). However, note that the length of the catalytically active part of the column was only 2 mm (column volume of ~14 mm^3). As a result, the contact time of the passing 4-NP medium with the catalyst was thus only between 1 and 4 s at given flow rates, which was still sufficient to convert 4-NP to 4-AP from more than 90 % in all cases. The decrease in TOF compared to bare $AuDAC$ nanoparticles can be attributed to the difference in the employed setup and the reduction of the catalytically active surface due to the bonding of $AuDAC$ to the $CHIT$ substrate.

Compared with other works, the obtained TOF values are similar to TOF = 0.33 min^{-1} found by (**Gopiraman et al., 2018**) for $AuNPs$ supported on cellulose nanofibers. However, it is essential to

recognize that the TOF reported by (**Gopiraman et al., 2018**) was determined using a different experimental setup, i.e., by stirring a defined amount of the prepared catalyst in the reaction medium. This setup enables direct interaction of the catalyst with the entire volume of the reaction mixture at once and is not limited by flow rate. Consequently, it leads to more effective catalysis, but the catalyst must be recovered after each cycle by centrifugation, which leads to unavoidable losses and possible product contamination. In contrast, the $AuCHIT$ catalytic column is directly reusable, as evidenced by the repeated catalytic experiments at different flow rates (three repeats for each flow rate, nine in total, see **Fig. 6**G). The catalytic efficacy even slightly increases throughout the three cycles for each flow rate, which can be explained by the partial swelling of $AuCHIT$_F during the procedure. Nevertheless, differences are minor, and the reproducibility of these catalytic experiments is thus very high.

4. Conclusions

The main goal of this contribution was to investigate the preparation of $AuNPs$ using fully oxidized DAC and to utilize the highly reactive $-CHO$ groups in the $AuDAC$ shell for affinity anchoring to chitosan nanofibers. In the first step, it was found that fully oxidized DAC is capable of near-instantaneous AuIn salt reduction and subsequent stabilization of formed AuNPs. This is a highly significant advantage compared to $AuNPs$ synthesis based on native polysaccharides, which often require several hours of synthesis. The resulting nanoparticles, with a spherical (polyhedral) shape and a size of approximately 5 nm (r_h = ∼20 nm), were subsequently used to form composites through the formation of Schiff bases between $-CHO$ groups of $AuDAC$ and $-NH_2$ groups of chitosan. This process, termed "affinity anchoring", proved to be much more effective than classic dip coating methods and led to the quantitative deposition of $AuNPs$. The stability of the $AuCHIT$ composite was further enhanced by reductive amination of imine bonds between $AuDAC$ or DAC remaining in the reaction mixture and chitosan, resulting in stability over a wide pH range from 3 to 9.

The catalytic efficiency of $AuDAC$ and $AuCHIT$ was tested on catalyzed reduction of 4-NP to 4-AP. The catalytic activity of $AuDAC$ was found to be significantly higher compared to related dicarboxy polysaccharides. The $AuCHIT$ composite material was also tested using a model catalytic device and found to be directly reusable, with catalytic activity comparable to those reported by other groups.

Furthermore, the modification potential of $AuDAC$ and its affinity towards amines open up new possibilities beyond the catalysis field, particularly in biomedical applications such as the development of therapeutic agents, biosensors, or attachment of targeting vectors for drug delivery. Future research may also explore different kinds of metal nanoparticles that could be prepared using this approach and affinity-anchored to any substrates containing amine or even amide groups, further expanding the ideas proposed above.

References

Archana, M., Sreekutty, J., Syama, H., Joseph, M. M., Anusree, K., Unnikrishnan, B., ... Sreelekha, T. (2023). Polysaccharide guided tumor delivery of therapeutics: A biofabricated galactomannan-gold nanosystem for augmented cancer therapy. Journal of Drug Delivery Science and Technology, 80, 104172. **https://doi.org/10.1016/j. jddst.2023.104172**

Bhatti, M. M., Anwar Bég, O., Ellahi, R., Doranehgard, M. H., & Rabiei, F. (2022). Electromagnetohydrodynamics hybrid nanofluid flow with gold and magnesium oxide nanoparticles

through vertical parallel plates. Journal of Magnetism and Magnetic Materials, 564, 170136. **https://doi.org/10.1016/jjmmm.2022.170136**

Cao, G., & Wang, Y. (2011). Nanostructures and nanomaterials: Synthesis, properties, and applications. In (2nd ed.), Vol. 2. World scientific. **https://doi.org/10.1142/7885**

Chakravarthi, S. S., Robinson, D. H., & De, S. (2007). Nanoparticles prepared using natural and synthetic polymers. In D. Thassu, M. Deleers, & Y. Pathak (Eds.), Nanoparticulate drug delivery systems (1st ed., pp. 51-60). CRC Press. **https://doi.org/ 10.1201/9781420008449-3**.

Chen, H., Kou, X., Yang, Z., Ni, W., & Wang, J. (2008). Shape- and size-dependent refractive index sensitivity of gold nanoparticles. Langmuir, 24(10), 5233-5237. **https://doi.org/10.1021/la800305j**

Cheng, H.-H., Chen, F., Yu, J., & Guo, Z.-X. (2017). Gold-nanoparticle-decorated thermoplastic polyurethane electrospun fibers prepared through a chitosan linkage for catalytic applications. Journal of Applied Polymer Science, 134(1). **https://doi.org/ 10.1002/app.44336**

Corma, A., & Garcia, H. (2008). Supported gold nanoparticles as catalysts for organic reactions. Chemical Society Reviews, 37(9), 2096. **https://doi.org/10.1039/b707314n**

Du, Y., Luo, X.-L., Xu, J.-J., & Chen, H.-Y. (2007). A simple method to fabricate a chitosan-gold nanoparticles film and its application in glucose biosensor. Bioelectrochemistry, 70(2), 342-347. **https://doi.org/10.1016/). bioelechem.2006.05.002**

Enustun, B. V., & Turkevich, J. (1963). Coagulation of colloidal gold. Journal of the American Chemical Society, 85(21), 3317-3328. **https://doi.org/10.1021/ ja00904a001**

Fahim, N., Ouyang, Z., Zhang, Y., Jia, B., Shi, Z., & Gu, M. (2012). Efficiency enhancement of screen-printed multicrystalline silicon solar cells by integrating gold nanoparticles via a dip coating process. Optical Materials Express, 2(2), 190. **https:// doi.org/10.1364/OME.2.000190**

Fernandes Queiroz, M., Melo, K., Sabry, D., Sassaki, G., & Rocha, H. (2014). Does the use of chitosan contribute to oxalate kidney stone formation? Marine Drugs, 13(1), 141-158. **https://doi.org/10.3390/md13010141**

Gao, C., Wang, S., Liu, B., Yao, S., Dai, Y., Zhou, L., Qin, C., & Fatehi, P. (2021). Sustainable chitosan-dialdehyde cellulose nanocrystal film. Materials, 14(19), 5851. **https://doi.org/10.3390/ma14195851**

Gomathi, P., Ragupathy, D., Choi, J. H., Yeum, J. H., Lee, S. C., Kim, J. C., . Ghim, H. D. (2011). Fabrication of novel chitosan nanofiber/gold nanoparticles composite towards improved performance for a cholesterol sensor. Sensors and Actuators B: Chemical, 153(1), 44-49. **https://doi.org/10.1016/j.snb.2010.10.005**

Gopiraman, M., Deng, D., Saravanamoorthy, S., Chung, I.-M., & Kim, I. S. (2018). Gold, silver and nickel nanoparticle anchored cellulose nanofiber composites as highly active catalysts for the rapid and selective reduction of nitrophenols in water. RSC Advances, 8(6), 3014-3023. **https://doi.org/10.1039/C7RA10489H**

Gupta, V. K., Kumar, S., Kukreja, R., & Chander, N. (2023). Experimental thermal performance investigation of a direct absorption solar collector using hybrid nanofluid of gold nanoparticles with natural extract of Azadirachta Indica leaves. Renewable Energy, 202, 1021-1031. **https://doi.org/10.1016/j.renene.2022.12.014**

Hasanova, N., £elik, S. E., & Apak, R. (2022). Dithioerythritol functionalized gold nanoparticles—based fluorometric sensing of biogenic amines in food samples. Journal of Food Composition and Analysis, 114, 104837. **https://doi.org/10.1016/j. jfca.2022.104837**

He, H., Chen, R., Zhang, L., & Shen, W. (2020). Growth of gold nanoparticles on cellulose nanofibers. Cellulose, 27(9), 5041-5053. **https://doi.org/10.1007/s10570-020-03142-5**

Heinert, D., & Martell, A. E. (1962). Pyridoxine and pyridoxal analogs. V. Syntheses and infrared spectra of Schiff bases. Journal of the American Chemical Society, 84(17), 3257-3263. **https://doi.org/10.1021/ja00876a009**

Kim, U.-J., Kim, H. J., Choi, J. W., Kimura, S., & Wada, M. (2017). Cellulose-chitosan beads crosslinked by dialdehyde cellulose. Cellulose, 24(12), 5517-5528. **https://doi. org/10.1007/s10570-017-1528-y**

Kim, U.-J., Kuga, S., Wada, M., Okano, T., & Kondo, T. (2000). Periodate oxidation of crystalline cellulose. Biomacromolecules, 1(3), 488-492. **https://doi.org/10.1021/ bm0000337**

Kim, U.-J., Wada, M., & Kuga, S. (2004). Solubilization of dialdehyde cellulose by hot water. Carbohydrate Polymers, 56(1), 7-10. **https://doi.org/10.1016/j. carbpol.2003.10.013**

Kozuch, S., & Martin, J. M. L. (2012). "Turning over" definitions in catalytic cycles. ACS Catalysis, 2(12), 2787-2794. **https://doi.org/10.1021/cs3005264**

Li, J., Wu, J., Zhang, X., Liu, Y., Zhou, D., Sun, H., . Yang, B. (2011). Controllable synthesis of stable urchin-like gold nanoparticles using hydroquinone to tune the reactivity of gold chloride. The Journal of Physical Chemistry C, 115(9), 3630-3637. **https://doi.org/10.1021/jp1119074**

Li, S., Zhang, L., Wang, T., Li, L., Wang, C., & Su, Z. (2015). The facile synthesis of hollow Au nanoflowers for synergistic chemo-photothermal cancer therapy. Chemical Communications, 51 (76), 14338-14341. **https://doi.org/10.1039/C5CC05676D**

Liu, F.-K., Chang, Y.-C., Ko, F.-H., Chu, T.-C., & Dai, B.-T. (2003). Rapid fabrication of high quality self-assembled nanometer gold particles by spin coating method. Microelectronic Engineering, 67-68, 702-709. **https://doi.org/10.1016/S0167-9317 (03)00175-8**

Liu, J., Kan, C., Shi, D., Ke, S., & Liu, Y. (2017). Stable silica-coated self-assembly of gold nanorods: Synthesis and plasmonic properties. Superlattices and Microstructures, 110, 191-197. **https://doi.org/10.1016Zj.spmi.2017.08.045**

Maddaloni, M., Alessandri, I., & Vassalini, I. (2022). Food-waste enables carboxylated gold nanoparticles to completely abat hexavalent chromium in drinking water. Environmental Nanotechnology, Monitoring & Management, 18, 100686. **https://doi. org/10.1016/j.enmm.2022.100686**

Medina, C., Santos-Martinez, M. J., Radomski, A., Corrigan, O. I., & Radomski, M. W. (2007). Nanoparticles: Pharmacological and toxicological significance: Nanoparticles. British Journal of Pharmacology, 150(5), 552-558. **https://doi.org/ 10.1038/sj.bjp.0707130**

Mizrahy, S., & Peer, D. (2012). Polysaccharides as building blocks for nanotherapeutics. Chemical Society Reviews, 41(7), 2623-2640. **https://doi.org/10.1039/C1CS15239D**

Muchová, M., Münster, L., Vávrová, A., Capáková, Z., Kuřitka, I., & Vícha, J. (2022). Comparison of dialdehyde polysaccharides as crosslinkers for hydrogels: The case of poly(vinyl alcohol). Carbohydrate Polymers, 279, 119022. **https://doi.org/10.1016/j. carbpol.2021.119022**

Münster, L., Capáková, Z., Fišera, M., Kuřitka, I., & Vícha, J. (2019). Biocompatible dialdehyde cellulose/poly(vinyl alcohol) hydrogels with tunable properties. Carbohydrate Polymers, 218, 333-342. **https://doi.org/10.1016/j. carbpol.2019.04.091**

Münster, L., Fojtů, M., Capáková, Z., Muchová, M., Musilová, L., Vaculovič, T., Balvan, J., Kuřitka, I., Masařík, M., & Vícha, J. (2021). Oxidized polysaccharides for anticancer-drug delivery: What is the role of structure? Carbohydrate Polymers, 257, 117562. **https://doi.org/10.1016/j.carbpol.2020.117562**

Münster, L., Fojtů, M., Capáková, Z., Vaculovič, T., Tvrdoňová, M., Kuřitka, I., Masařík, M., & Vícha, J. (2019). Selectively oxidized cellulose with adjustable molecular weight for controlled release of platinum anticancer drugs. Biomacromolecules, 20(4), 1623-1634. **https://doi.org/10.1021/acs. biomac.8b01807**

Münster, L., Hanulíková, B., Machovský, M., Latečka, F., Kuřitka, I., & Vícha, J. (2020). Mechanism of sulfonation-induced chain scission of selectively oxidized polysaccharides. Carbohydrate Polymers, 229, 115503. **https://doi.org/10.1016/j. carbpol.2019.115503**

Münster, L., Vícha, J., Klofáč, J., Masař, M., Kucharczyk, P., & Kuřitka, I. (2017). Stability and aging of solubilized dialdehyde cellulose. Cellulose, 24(7), 2753-2766. **https:// doi.org/10.1007/s10570-017-1314-x**

Qiu, Y., Ma, Z., & Hu, P. (2014). Environmentally benign magnetic chitosan/Fe3O4 composites as reductant and stabilizer for anchoring Au NPs and their catalytic reduction of 4-nitrophenol. Journal of Materials Chemistry A, 2(33), 13471-13478. **https://doi.org/10.1039/C4TA02268H**

Rajeshkumar, S., Malarkodi, C., Al Farraj, D. A., Soliman Elshikh, M., & Mohana Roopan, S. (2021). Employing sulphated polysaccharide (fucoidan) as medium for gold nanoparticles preparation and its anticancer study against HepG2 cell lines. Materials Today Communications, 26, 101975. **https://doi.org/10.1016/j. mtcomm.2020.101975**

Regiel-Futyra, A., Kus-Liśkiewicz, M., Sebastian, V., Irusta, S., Arruebo, M., Stochel, G., & Kyziol, A. (2015). Development of noncytotoxic chitosan-gold nanocomposites as efficient antibacterial materials. ACS Applied Materials & Interfaces, 7(2), 1087-1099. **https://doi.org/10.1021/am508094e**

Sadanandan, S., Meenakshi, V. S., Ramkumar, K, Pillai, N. P., Anuvinda, P., Sreelekshmi, P. J., ... Sreejaya, M. M. (2023). Biorecognition elements appended gold nanoparticle biosensors for the detection of food-borne pathogens—A review. Food Control, 148, 109510. **https://doi.org/10.1016/j.foodcont.2022.109510**

Schmidbaur, H., Raubenheimer, H. G., & Dobrzanáska, L. (2014). The gold-hydrogen bond, Au-H, and the hydrogen bond to gold, Au—H-X. Chemical Society Reviews, 43 (1), 345-380. **https://doi.org/10.1039/C3CS60251F**

Spedding, H. (1960). Infrared spectra of periodate-oxidised cellulose. Journal of the Chemical Society (Resumed), 3147-3152. **https://doi.org/10.1039/jr9600003147**

Straka, M., Andris, E., Vícha, J., Růžička, A., Roithová, J., & Rulíšek, L. (2019). Spectroscopic and computational evidence of intramolecular $Au^{1}\cdots H^{+}$—N hydrogen bonding. Angewandte Chemie, 131(7), 2033-2038. **https://doi.org/10.1002/ ange.201811982**

Swierczewska, M., Han, H. S., Kim, K., Park, J. H., & Lee, S. (2016). Polysaccharide-based nanoparticles for theranostic nanomedicine. Advanced Drug Delivery Reviews, 99, 70-84. **https://doi.org/10.1016/j.addr.2015.11.015**

Tiwari, P., Vig, K, Dennis, V., & Singh, S. (2011). Functionalized gold nanoparticles and their biomedical applications. Nanomaterals, 1(1), 31-63. **https://doi.org/10.3390/ nano1010031**

Vávrová, A., Capáková, T., Kuřitka, I., Vícha, J., & Münster, L. (2022). One-step synthesis of gold nanoparticles for catalysis and SERS applications using selectively dicarboxylated cellulose and hyaluronate. International Journal of Biological Macromolecules, 206, 927-938. **https://doi.org/10.1016/j.ijbiomac.2022.03.043**

Wang, C., Gao, X., Chen, Z., Chen, Y., & Chen, H. (2017). Preparation, characterization and application of polysaccharide-based metallic nanoparticles: A review. Polymers, 9(12), 689. **https://doi.org/10.3390/polym9120689**

Wunder, S., Polzer, F., Lu, Y., Mei, Y., & Ballauff, M. (2010). Kinetic analysis of catalytic reduction of 4-nitrophenol by metallic nanoparticles immobilized in spherical polyelectrolyte brushes. The Journal of Physical Chemistry C, 114(19), 8814-8820. **https://doi.org/10.1021/jp101125j**

Xiao, T., Huang, J., Wang, D., Meng, T., & Yang, X. (2020). Au and Au-based nanomaterials: Synthesis and recent progress in electrochemical sensor applications. Talanta, 206, 120210. **https://doi.org/10.1016/j.talanta.2019.120210**

Yuan, P., Liu, L., Aipire, A., Zhao, Y., Cai, S., Wu, L., Yang, X., Aimaier, A., Lu, J., & Li, J. (2023). Evaluation and mechanism of immune enhancement effects of Pleurotus ferulae polysaccharides-gold nanoparticles. International Journal of Biological Macromolecules, 227, 1015-1026. **https://doi.org/10.1016/j.ijbiomac.2022.11.277**

Yuan, X., Ge, L., Zhou, H., & Tang, J. (2023). Size, composition, and surface capping-dependent catalytic activity of spherical gold nanoparticles. Spectrochimica Acta Part A: Molecular and Biomolecular Spectroscopy, 287, 122082. **https://doi.org/10.1016/j. saa.2022.122082**

Yue, Y., Yokota, Y., & Uchihashi, T. (2023). Biosynthesis of highly branched gold nanoparticles through structural engineering of fatty acids. IScience, 26(1), 105864. **https://doi.org/10.1016/j.isci.2022.105864**

Zhang, K., Shen, M., Liu, H., Shang, S., Wang, D., & Liimatainen, H. (2018). Facile synthesis of palladium and gold nanoparticles by using dialdehyde nanocellulose as template and reducing agent. Carbohydrate Polymers, 186, 132-139. **https://doi.org/ 10.1016/j.carbpol.2018.01.048**

Zhang, X. (2015). Gold nanoparticles: Recent advances in the biomedical applications. Cell Biochemistry and Biophysics, 72(3), 771-775. **https://doi.org/10.1007/s12013-015-0529-4**